Florian Mai*
Andreas Jess

CO_2 Conversion to Higher Hydrocarbons on Iron-Based Catalysts: Promoter Impact and Kinetic Studies

Promoted iron catalysts were tested for their Fischer–Tropsch (FT) activity to convert CO_2/H_2, CO/H_2 and their mixtures to higher hydrocarbons (220 °C–300 °C, 20 bar, $H_2/(CO_2+CO) = 3$). The results show that iron-sintered catalysts are able to convert CO_2 at moderate conditions to higher hydrocarbons (HCs) with a still low methane selectivity. Kinetic studies showed that CO_2 is not directly converted to higher HCs but at first reduced by H_2 to CO followed by FTS of CO. For a pure CO_2/H_2 mixture and a CO_2 conversion of 10% (220 °C), the FeCuZnK catalyst has the highest C_{2+} selectivity (57 wt_C%), the lowest methane selectivity (10 wt_C%), and 32% of CO_2 are converted to the intermediate CO. At 300 °C and a higher CO_2 conversion of 47%, the C_{2+} selectivity is even 73 wt_C% (methane 19 wt_C%, methanol 4 wt_C%, and 4 wt_C% CO).

This is an open access article under the terms of the Creative Commons Attribution License, which permits use, distribution and reproduction in any medium, provided the original work is properly cited.

Supporting Information available online

Keywords: CO_2 hydrogenation, Fischer–Tropsch synthesis, Iron

Received: January 13, 2025; *revised:* February 14, 2025; *accepted:* February 20, 2025

DOI: 10.1002/ceat.12010

1 Introduction

A major challenge to mitigate the effects of climate change is the sustainable production of liquid fuels from renewable resources to decrease anthropogenic CO_2 emissions. One option is the use of CO_2 from various sources (power plants, chemical industry, and possibly separated from air) and subsequent conversion with renewable hydrogen to higher hydrocarbons (HCs). The preferred objective of this process is the production of liquid products such as diesel oil for trucks and jet fuel, which are currently difficult or impossible to substitute by the use of electrical energy or electrically powered transport.

For the activation and conversion of CO_2 into higher HCs, conventional power-to-liquid (PtL) plants may be used. However, such CO_2-based PtL systems (today only realized in small scale units [1]) mediated by Fischer–Tropsch synthesis (FTS) will according to today´s knowledge include a two-stage system with the conversion of CO_2 and H_2 into CO (and H_2O) by the reverse-water-gas-shift reaction (RWGS) and the subsequent FTS of the produced syngas ($CO + 2\,H_2 \rightarrow -CH_2- + H_2O$; CH_2 represents a methylene group in a paraffinic HC). In consequence, higher HCs are currently only synthesized on a commercial scale (South Africa, Qatar) by FTS, that is, based on CO and syngas produced from coal or natural gas [2, 3].

The hydrogenation of CO_2 to HCs (formally $CO_2 + 3\,H_2 \rightarrow CH_2 + 2\,H_2O$) at moderate FTS temperatures of about 220 °C is today limited to a conversion of only up to 15%. The main reason is the endothermic, thermodynamically limited RWGS reaction, which is favored by high temperatures. Since FTS may substantially convert CO formed by RWGS, higher conversions of CO_2 are in principle possible. A suitable catalyst should therefore show both, a high activity for RWGS and a similar or even higher activity for FTS. Furthermore, the catalyst should have a low selectivity to methane.

Note for clarity: In this work and throughout most of the literature, the term FTS is only related to the reaction of CO and H_2 to HCs, whereas the "indirect" synthesis starting from CO_2 is named as CO_2 hydrogenation (to HCs), as it is—as also shown in this work—basically related to CO formation by RWGS followed by subsequent FTS.

Many studies show that one potential way to directly convert CO_2 with H_2 to higher HCs is the use of iron-based catalysts [4–6]. They contain different active sites (iron oxides and iron carbides) which perform the two main catalytic reactions (RWGS and FTS) simultaneously as shown in Fig. 1. The FTS takes place on iron carbides, according to Ref. [7], and leads to the formation of a variety of HCs following the Anderson–Schulz–Flory distribution (ASF), which is (with the exception of methane formation) governed by the chain growth probability α. Direct methanation of CO_2 may occur as a side reaction.

In this work, the single and combined effects of the promoters Cu, Zn, and K on a sintered iron catalyst on CO_2 hydrogenation were investigated. At first, a pure iron catalyst was used. Afterward a single promoter (Cu or Zn), promoter pair (Cu/Zn) or even three promoters (Cu, Zn, and K) were incorporated. The studies with each catalyst include the measurements of activity, selectivity and stability and were carried out with different $H_2/CO_2/CO$ mixtures (including pure CO and pure CO_2 as

Florian Mai (Florian.Mai@uni-bayreuth.de), Prof. Dr.-Ing. Andreas Jess
Faculty of Engineering, Center of Energy Technology, University of Bayreuth, Universitätsstraße 30, 95447, Bayreuth, Germany.

 © 2025 The Author(s). Chemical Engineering & Technology published by Wiley-VCH GmbH

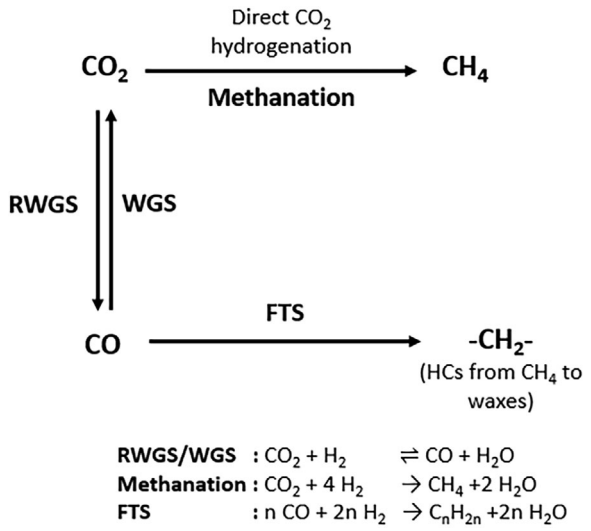

Figure 1. Reaction scheme of the reverse water-gas-shift reaction, the Fischer–Tropsch process and the direct methanation of CO_2 on an iron-based catalyst. It should be noted that the route of methanation is only relevant for catalysts without potassium, as will be demonstrated subsequently.

carbon source) and also at a varying CO_2 conversion, thereby even at a high temperature of 300 °C.

2 Materials and Methods

2.1 Catalyst Preparation

The catalysts are based on sintered iron catalysts and were synthesized according to Ref. [8]. About 50 g of the metal oxides (ZnO, Fe_2O_3, and CuO) were mixed and ball-milled (Pulverisette 5) with 60 ZrO_2 balls (10 mm) in a ZrO_2 container with cyclohexane as solvent. The milling procedure were 30 min (6 × 5 min milling with 20 min break in between) at 400 rpm. After drying, a mixture of water and potassium carbonate (K_2CO_3) were added, then dried again at 110 °C in an oven. The powders were sintered in a muffle furnace at 1100 °C (10 °C min^{-1}) for 90 minutes, crushed and sieved to particles below 180 µm. The catalyst names reflect the quantity of promoters, for example, 100Fe15Cu5Zn5K, where numbers indicate the weight proportion of each element relative to iron.

2.2 Catalyst Characterization

The composition of the unreduced catalysts was determined by inductively coupled plasma optical emission spectroscopy (ICP-OES, Optima 7300 DV, PerkinElmer). About 0.1 g of catalyst were added to 8 mL of aqua regia (HCl/HNO_3 = 3 (m/m)) in a Teflon container and decomposed in a high-pressure microwave-assisted oven (Multiwave 3000, Anton Paar). The samples were diluted with 50 mL of deionized water and 2% HNO_3 prior to ICP-OES measurement.

The surface area was determined by N_2 adsorption at –196 °C (Micromeritics Gemini V) and evaluated by the BET method in a pressure range of $p/p_0 = 0.05$–0.3. In advance, the catalyst (approx. 0.5 g) was degassed at 100 °C for 16 h to remove any adsorbed surface species. The results of the catalyst characterization can be found in the Supporting Information (SI).

2.3 Catalytic Testing: Evaluation of Activity and Selectivity of the Catalyst

The catalytic testing of the CO/CO_2 conversion and selectivity to different products (mainly HCs) was measured in a lab-scale tubular reactor setup, consisting of a stainless steel fixed-bed reactor (14 mm inner diameter) surrounded by an aluminum block to ensure isothermal conditions in the catalyst bed. The heating is realized by an electrical heating jacket. Gas flows (N_2, CO, CO_2, H_2, and 1% cyclopropane in N_2) were controlled by mass flow controllers and cyclopropane served as an internal standard for online gas chromatography. The total pressure of the system was controlled by a back-pressure regulator. A process flow diagram can be found in the SI. For the experiments, about 7.5 g of catalyst were diluted with about 32 g of silica sand (particle size 210–300 µm). The catalysts were reduced by heating to 360 °C at 2 °C/min with a holding period of 120 min at 360 °C (20% H_2 in N_2, $\dot{V} = 20$ nL/h). Afterward the gas was switched to pure H_2 with a flow of 20 nL/h at 360 °C for 120 min to complete the reduction process. At the end of the reduction, the catalysts were cooled under N_2 atmosphere to room temperature. Thereafter, the reactor was pressurized to 20 bar under $H_2/CO = 2$ (V/V) atmosphere and then heated to the reaction temperature (220 °C). Since iron catalysts undergo a structural change and form iron carbides under FTS conditions, they were treated for 72 h prior to the kinetic measurements.

The in- and outlet concentrations of CO, CO_2, and H_2 were measured by a gas analyzer (Emerson X-Stream XE) equipped with infrared detectors (IR) and a thermal conductivity detector (TCD) for hydrogen. The values of the gaseous products (C_1–C_6) were analyzed using online GC samples (Perkin Elmer Clarus 690 equipped with a Rtx-100-DHA capillary column and a flame ionization detector (FID)). The liquid and (at 20 °C) solid products (waxes) were collected by cooling traps (25 °C, 0 °C, –79 °C) and analyzed using two offline GCs (Bruker 450-GC and Agilent Technologies 7890B). These were equipped with an Ultra 2 column (liquid products) and an VF-5ht UltiMetal column (waxes). FID's were used in both cases. Cyclooctane was used as an internal standard in the liquid sample. The wax products were extracted directly from the cold trap and weighed afterward. The performance of the catalyst was evaluated under steady state conditions (24 h on stream) and the total mass balance (wt_C%) was maintained within 100 ± 5% to ensure reliability throughout the experiments.

2.3.1 Calculations

The reaction rate of CO or CO_2 is calculated by Equation 1.

$$r_i = \frac{\dot{n}_{i,in} - \dot{n}_{i,out}}{m_{cat}} \quad (1)$$

 © 2025 The Author(s). Chemical Engineering & Technology published by Wiley-VCH GmbH

15214125, 2025, 4, Downloaded from https://onlinelibrary.wiley.com/doi/10.1002/ceat.12010 by Universitaet Bayreuth, Wiley Online Library on [10/03/2026]. See the Terms and Conditions (https://onlinelibrary.wiley.com/terms-and-conditions) on Wiley Online Library for rules of use; OA articles are governed by the applicable Creative Commons License

with i as either CO or CO_2. The conversion of CO or CO_2 is given by

$$X_i = \frac{\dot{n}_{i,in} - \dot{n}_{i,out}}{\dot{n}_{i,in}} \tag{2}$$

In case of $H_2/CO_2/CO$ experiments, the combined conversion of CO_2 and CO is calculated by Equation 3.

$$X_{CO_x} = \frac{\left(\dot{n}_{CO_2,in} + \dot{n}_{CO,in}\right) - \left(\dot{n}_{CO_2,out} + \dot{n}_{CO,out}\right)}{\left(\dot{n}_{CO_2,in} + \dot{n}_{CO,in}\right)} \tag{3}$$

The selectivity to CO is given by Equation 4. The selectivity to CO_2 is calculated in the same way, only the indices (CO, CO_2) as shown in the equation are swapped.

$$S_{CO} = \frac{\dot{n}_{CO,out}}{\dot{n}_{CO_2,in} - \dot{n}_{CO_2,out}} \tag{4}$$

The hydrocarbon selectivities were determined by the Equations 5 and 6 with regard to CO_2 hydrogenation.

$$S_{C_n} = \frac{\dot{m}_{C_n}}{\dot{m}_{C_CO_2,in} - \dot{m}_{C_CO_2,out} - \dot{m}_{C_CO,out}} \quad (n = 1,\ 2,\ 3,\ 4\ldots) \tag{5}$$

$$S_{C_{5+}} = 1 - S_{CH_4} - S_{C_2} - S_{C_3} - S_{C_4} \tag{6}$$

It should be noted that the selectivities are based on the carbon content of the product by weight. Consequently, the selectivities are therefore given in wt_C%. The calculation of the chain growth probability α is explained in detail in the SI.

For comparability of experiments, the modified residence time τ_{mod} is used

$$\tau_{mod} = \frac{m_{Cat}}{\dot{V}_{total}(p, T)} \tag{7}$$

with STP as standard temperature and pressure ($T_{STP} = 273.15$ K, $p_{STP} = 1.013$ bar).

For a constant CO_x conversion (here mostly 10%), τ_{mod} is also a good measure of the reaction rate; that is, a high value reflects a low rate and vice versa.

2.3.2 Kinetic Model (Used for the FeCuZnK Catalyst)

The fundamental reactions (and assumptions for our kinetic model) are that the RWGS reaction (CO_2 shift) is followed by the FT reaction; that is, HCs are not directly formed from CO_2. The form of rate equations for these reactions are shown in Equations 8 and 9, showing that equations according to the Langmuir–Hinshelwood–Hougen–Watson (LHHW) mechanism were utilized [3]. Riedel et al. proposed similar rate equations in a previous study [7], and the principle structure was here also used but adapted with regard to the values of kinetic parameters (a, b, c, etc.). Note that this kinetic model was only used for FeCuZnK catalyst, which turned out (as shown below) to be the by far best catalyst to convert a CO_2 rich syngas to valuable liquid HCs. The direct CO_2 hydrogenation pathway is not included in the model, as methanation on FeCuZnK is suppressed.

$$r_{RWGS} = k_{RWGS} * \frac{\left(c_{CO_2} * c_{H_2} - \left(\frac{c_{CO} * c_{H_2O}}{K_{eq}}\right)\right)}{1 + a_{1,H_2O} * c_{H_2O} + b_{1,CO_2} * c_{CO_2} + c_{1,CO} * c_{CO}} \tag{8}$$

$$r_{FTS} = k_{FTS} * \frac{c_{CO} * c_{H_2}}{1 + a_{2,H_2O} * c_{H_2O} + b_{2,CO_2} * c_{CO_2} + c_{2,CO} * c_{CO}} \tag{9}$$

The effect of the chemical equilibrium limitation of the RWGS reaction as shown in Equation 8 is considered by the equilibrium constant K_{eq}, Equation 10, as proposed by Graaf et al. [9].

$$K_{eq} = 10^{\left(\frac{-2073}{T(K)} + 2.029\right)} \tag{10}$$

The inhibition parameters a_{n,H_2O}, b_{n,CO_2} and $c_{n,CO}$ ($n = 1,2$) were determined by adjusting the calculated values of the reaction rates to the experimental results. In an iterative procedure, the sum of square errors in the differences between the CO_2 conversion and CO selectivities (experimental and model) was minimized. The values of the inhibition parameters and the activation energy can be found in the SI.

3 Results

3.1 Performance of Catalysts at Varying Carbon Dioxide/Carbon Monoxide Ratio (CO_2/CO)

The individual and combined effects of Cu, Zn, and K on iron-based sintered catalysts with pure H_2/CO_2 and mixtures of $H_2/CO_2/CO$ at a constant molar H_2/CO_x ratio of three at a fixed temperature of 220 °C were investigated. The experiments were carried out at around $X_{CO_x} = 10\%$ (Equation 3), so the modified residence time was adjusted. The objective was to determine the extent to which the catalysts still convert CO_2 at an increasing CO concentration, as the ability of the catalysts to achieve a high CO_2 conversion in the presence of both CO_2 and CO at elevated CO concentrations is a crucial factor in determining their active and selectivity performance. Different CO_2/CO ratios were tested, and the results for a molar ratio of $H_2/CO_2/CO$ of 3/0.75/0.25 and pure H_2/CO_2 are presented in Fig. 2; the outcome for other $H_2/CO_2/CO$ ratios can be found in the SI.

In case of the pure iron catalyst (100Fe), the selectivities change by the addition of CO, as clearly indicated by the comparison shown in Fig. 2: The formation of C_2–C_4 paraffins increases, 45 wt_C% with CO_2 and CO compared to only 24 wt_C% with pure CO_2. The addition of CO to the reactant gas leads to a net CO_2 production by the water-gas-shift (WGS) reaction (7 wt_C%) in contrast to 24 wt_C% CO selectivity with pure H_2/CO_2, which indicates a preferential adsorption of CO over CO_2 on the catalyst surface. Furthermore, the pure iron catalyst shows overall the highest methane selectivity regardless of the CO_2/CO ratio with 45 wt_c % for pure H_2/CO_2 and 35 wt_C % by the addition of CO.

In case of only zinc as promoter (100Fe5Zn), there is a small but notable increase in the selectivity to long-chain products in

 © 2025 The Author(s). Chemical Engineering & Technology published by Wiley-VCH GmbH

15214125, 2025, 4, Downloaded from https://onlinelibrary.wiley.com/doi/10.1002/ceat.12010 by Universitaet Bayreuth, Wiley Online Library on [10/03/2026]. See the Terms and Conditions (https://onlinelibrary.wiley.com/terms-and-conditions) on Wiley Online Library for rules of use; OA articles are governed by the applicable Creative Commons License

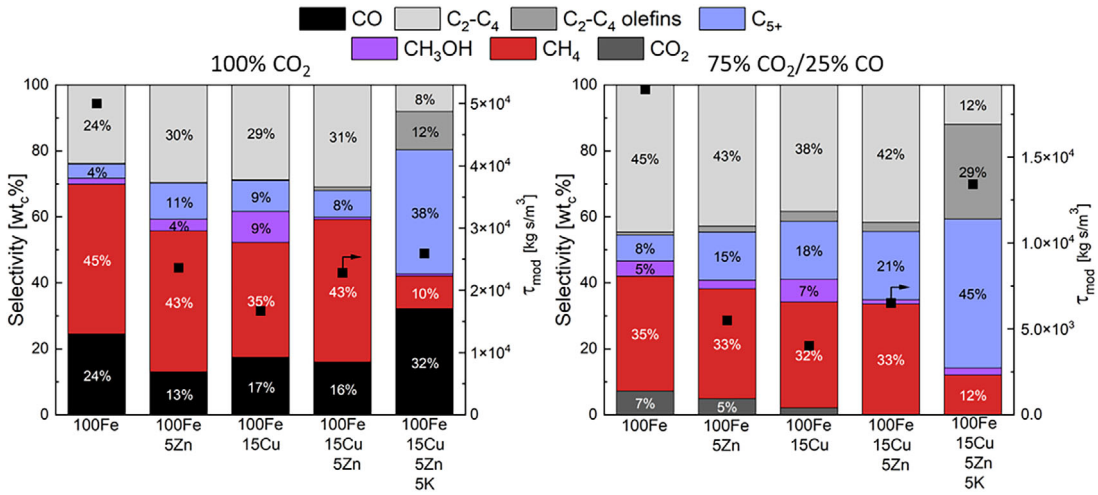

Figure 2. Selectivities to CO_2, CO, and HCs for each catalyst for pure H_2/CO_2 (left) and a $H_2/CO_2/CO$ ratio of 3/0.75/0.25 (right) (values < 3 wt_c% not displayed with numbers). τ_{mod} is shown by datapoints. Conditions: $m_{cat} = 7.5$ g, $X_{CO_x} \approx 10\%$, $\frac{H_2}{CO_x} = 3(\frac{n}{n})$, TOS ≈ 24 h, 220 °C, $p = 20$ bar.

case of CO present in the syngas, 15 wt_C% C_{5+} and 43 wt_C% C_2-C_4 compared to 11 wt_C% and 30 wt_C% without CO, while CO_2 (5 wt_C%) is still produced by WGS. The incorporation of copper only (100Fe15Cu) continues to follow the trend toward a higher production of long-chain products and less (net) production of CO_2. However, the highest production of methanol 9 wt_C% (H_2/CO_2) and 7 wt_C% (addition of CO) of all catalysts are noteworthy. The methanol formation can be explained by the catalytic effects of Cu [7, 8].

For the 100Fe15Cu5Zn catalyst, there is not anymore, a net production of CO_2 when CO is added, but also no consumption of CO_2. This indicates that the added CO_2 is then almost an inert component and is neither consumed by RWGS nor generated by WGS. In addition, by combining Cu and Zn, the methanol formation gets suppressed to a negligible value of only 1 wt_C%. This is an interesting and unexpected effect because the conventional catalyst for methanol synthesis ($Cu/ZnO/Al_2O_3$) is made up of these elements used here as promoters. It can therefore be proposed that iron or zinc inhibits the formation of methanol within this particular configuration.

A comparison of the selectivities of the 100Fe15Cu5Zn5K catalyst in H_2/CO_2 atmosphere with the case of CO addition (Fig. 2) reveals a clear distinction and advantage of this catalytic system compared to pure Fe and the other catalysts. The addition of potassium has a significant positive impact on the HC selectivities. This catalyst exhibits the highest selectivity to C_2–C_4 olefins (12 wt_C% and 29 wt_C%) and long-chain hydrocarbons C_{5+} (38 wt_C% and 45 wt_C%) and the lowest selectivity to methane (10 wt_C% and 12 wt_C%). These values are comparable to similar unsupported catalysts in literature [10, 11]. This shift in selectivities is also observable in the chain growth probability. The 100Fe15Cu5Zn5K catalyst has the highest α values at 0.6 (α_{C3-C8}) and 0.92 ($\alpha_{C12-C25}$) for pure H_2/CO_2. The chain growth probabilities for the other catalysts are listed in the SI. Furthermore, no net formation of CO_2 takes place by the addition of CO, and, in contrast to the 100Fe15Cu5Zn catalyst, CO_2 and CO are both consumed. According to Dry et al., the electronic properties of potassium, when interacting with iron-based catalysts, result in enhanced CO_2 adsorption and reduced H_2 adsorption [12, 13]. This obviously leads here to an increased formation of CO (Fig. 2 left), which subsequently reacts to long-chain hydrocarbons and olefins under conditions of reduced H_2 concentration on the catalyst surface. Investigation by others with slightly different catalysts (FeK, FeCuK, FeZnK with higher K-content) resulted in a higher Olefin/Paraffin ratios (C_2–C_4) in the range of 3 to 7, in comparison to the O/P ratio in this work of 1.5. In contrast, lower C_{5+} selectivities and higher CH_4 selectivities were observed, consequently resulting in lower α values as in the present study [11, 14]. According to Choi et al. and Chen et al., a further increase in the K-content above 5 wt% significantly enhances the olefin production but also leads to shorter chains. The reason for this is the excess K on the catalyst surface, which enhances Fe-C bonds and carbon deposition therefore leading to a reduced catalyst stability [15, 16].

A comparison of the methane selectivity (determined experimentally and calculated using α) shows significant deviations at higher CO_2 contents for all catalysts except FeCuZnK. This indicates that direct CO_2 hydrogenation/methanation occurs to a certain extent for the catalysts without potassium. The comparison of the methane selectivities as a function of the CO_2 content is shown as an example for FeCuZnK and Fe in Fig. 3. The data for the other catalysts can be found in the SI.

Regarding the activity of the catalysts, promotion with potassium slightly decreases the activity compared to 100Fe15Cu5Zn (0.53 $mmol_{CO_2}$ $s^{-1}kg_{Cat}{}^{-1}$ and 0.44 $mmol_{CO_2}$ $s^{-1}kg_{Cat}{}^{-1}$ for 100Fe15Cu5Zn5K). Fig. 4 illustrates the experimental reaction rates (symbols: CO in red; CO_2 in black) and the model-based calculation of the rates as a function of the molar CO_2 content $n_{CO_2}/(n_{CO_2} + n_{CO})$ of the 100Fe15Cu5Zn5K catalyst. Up to a molar CO_2 content of about 70 mol-% within the CO_x-feed, the negative reaction rate for CO_2 indicates a (net) CO_2 production whereas from this concentration on CO_2 is consumed (at

 © 2025 The Author(s). Chemical Engineering & Technology published by Wiley-VCH GmbH

15214125, 2025, 4, Downloaded from https://onlinelibrary.wiley.com/doi/10.1002/ceat.12010 by Universitaet Bayreuth, Wiley Online Library on [10/03/2026]. See the Terms and Conditions (https://onlinelibrary.wiley.com/terms-and-conditions) on Wiley Online Library for rules of use; OA articles are governed by the applicable Creative Commons License

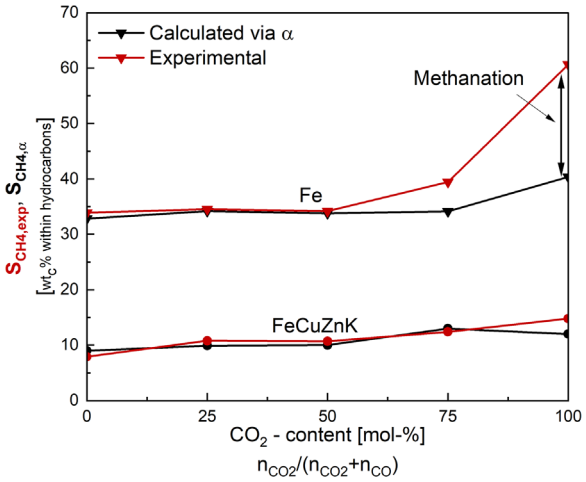

Figure 3. Methane selectivity (experimentally in red, calculated via α in black) for Fe and FeCuZnK depending on the CO_2/CO ratio (mol-%). Deviations of the calculated and experimentally measured values suggest a distinct reaction pathway for direct CO_2 hydrogenation/methanation that does not align with the FTS process.

65 mol-% according to the model). This (favorable) trend is not observed in any of the other catalysts. All data of the respective reaction rates of the remaining catalysts can be found in the SI.

Consequently, the 100Fe15Cu5Zn5K catalyst is the most efficient one for the conversion of CO_2 even in the presence of CO. This is a crucial attribute, as the recycling of the unreacted gas is essential for achieving an enhanced CO_2 conversion on an industrial scale.

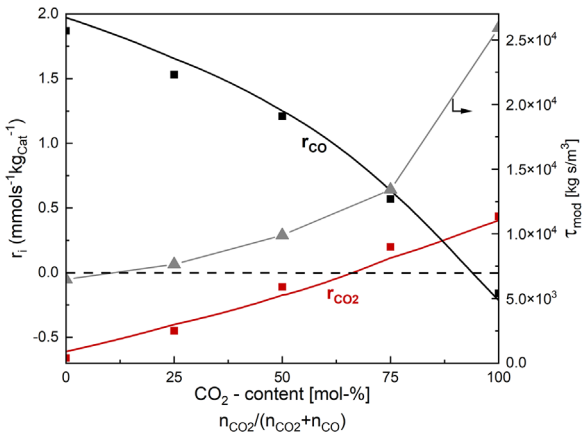

Figure 4. Reaction rates (CO black and CO_2 red) and τ_{mod} (gray triangles and line as guide for the eyes) depending on the CO_2/CO ratio (mol-%) with 100Fe15Cu5Zn5K. Lines for the rate are calculated with the kinetic model and symbols represent data points from experiments. Negative values indicate a net production of CO_2 and positive values a consumption. Conditions: $m_{cat} = 7.5$ g, $X_{CO_x} \approx 10\%$, $\frac{H_2}{CO_x} = 3(\frac{n}{n})$, TOS $\approx$ 24 h, 220 °C, $p = 20$ bar.

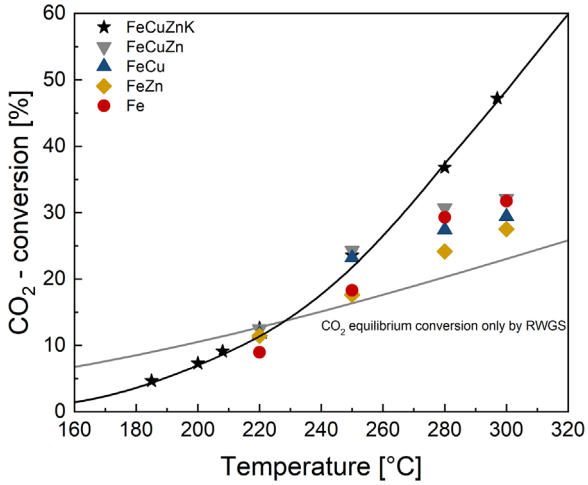

Figure 5. CO_2 conversion of each catalyst (symbols), CO_2 equilibrium conversion (thin gray line for only RWGS) and model data (black line) for the FeCuZnK catalyst at different temperatures. CO_2 equilibrium conversion calculated from the components H_2, CO_2, CO, and H_2O with the software HSC Chemistry 8 (Outotec Technologies), which is using the Gibbs energy minimization method. Conditions: $m_{cat} = 7.5$ g, $\frac{H_2}{CO_2} = 3(\frac{n}{n})$, TOS $\approx$ 24 h, 220–300 °C, $p = 20$ bar, $\tau_{mod,220°C} \approx 50{,}000$ kg$_{Kat}$sm^{-3}, $\tau_{mod,300°C} \approx 45{,}000$ kg$_{Kat}$sm^{-3}.

3.2 Performance of the Catalysts at a Varying CO_2 Conversion for Syngas Free of CO

The ability of the catalysts to achieve a high CO_2 conversion is an important aspect with regard to a technical synthesis of HCs based on CO_2 only or a CO_2 rich syngas, and is significantly influenced and determined by both the RWGS and FTS activity. However, the presence of significant quantities of water/steam in the system also represents a considerable inhibitory factor, as steam is formed to a high extent at a high degree of conversion of CO_x. Therefore, the catalysts were exposed to a constant flow rate of H_2 and CO_2 (i.e., a constant τ_{mod}), while the temperature was varied in four steps (220°–250 °C–280 °C–300 °C), with the exception of FeCuZnK, as then even lower temperatures were also tested in order to decrease the conversion of CO_2. Each catalyst was then re-exposed to 220 °C to rule out deactivation due to elevated temperatures. The CO_2 conversion profile as a function of temperature for syngas free of CO is illustrated in Fig. 5. Additionally, the CO_2 equilibrium conversion only achievable by RWGS (thin gray line) and the model-based calculation for 100Fe15Cu5Zn5K (black line) are shown.

At a low temperature (here 220 °C), the measured values remain in agreement with the equilibrium curve. However, as the temperature increases, the actual values of the CO_2 conversion deviate more and more from the theoretical values, clearly indicating that considerably higher CO_2 conversions are achieved by the subsequent FTS reaction converting CO formed by RWGS.

The 100Fe15Cu5Zn5K catalyst shows the highest CO_2 conversion under the specified reaction conditions. It is the only catalyst with an increase in CO_2 conversion with increasing temperature reaching a remarkable CO_2 conversion of 47% at 300 °C.

© 2025 The Author(s). Chemical Engineering & Technology published by Wiley-VCH GmbH

15214125, 2025, 4, Downloaded from https://onlinelibrary.wiley.com/doi/10.1002/ceat.12010 by Universitaet Bayreuth, Wiley Online Library on [10/03/2026]. See the Terms and Conditions (https://onlinelibrary.wiley.com/terms-and-conditions) on Wiley Online Library for rules of use; OA articles are governed by the applicable Creative Commons License

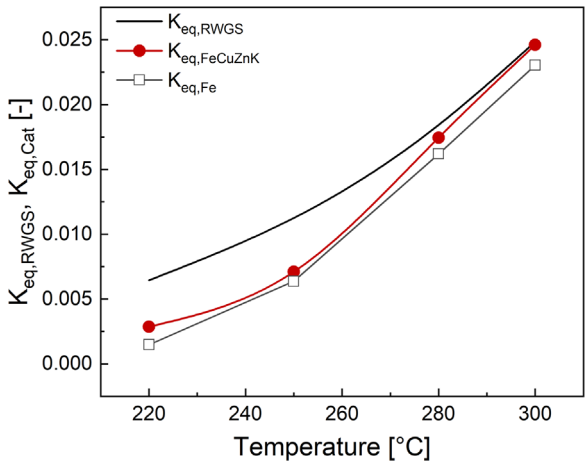

Figure 6. Equilibrium constant $K_{eq,RWGS}$ and experimental values of the respective ratio as function of temperature. $K_{eq,RWGS}$, according to Equation 10. Actual experimental $K_{eq,Cat}$ for 100Fe15Cu5Zn5K and 100Fe calculated based on the measured concentrations of CO_2, CO, H_2, and H_2O (symbols + line for interpolation) during stationary and stable operation at each temperature and CO_2 conversion.

All other catalysts show a maximum conversion of 30% or even lower at these temperatures. Similar unsupported catalysts reported in the literature achieved conversions of approximately 40% at 300 °C [17, 18].

At elevated temperatures (above 280 °C) all catalysts, except of the one containing potassium, show no significant increase in CO_2 conversion (Fig. 5). This is probably attributable to a specific form of inhibition or deactivation resulting from the increasing concentrations of H_2O at high CO_2 conversions. The impact of water on iron catalysts and their structure has been previously investigated, for example, by Claeys et al. [19]. This study demonstrates that significant quantities of water/steam can result in the oxidation of Hägg carbide (χ-Fe_5C_2) to magnetite (Fe_3O_4). Since iron carbides are mostly identified as the active phase for FTS in literature, a reduction in FTS activity was also observed with a decline in the carbide phase. The experiments show that the potassium promoted catalyst exhibits a higher tolerance to inhibition by water.

Fig. 6 compares the values of the equilibrium constant ($K_{eq,RWGS}$) of the RWGS at each temperature and the corresponding experimental (100Fe15Cu5Zn5K, 100Fe) values ($K_{eq,Cat}$) of this ratio as a function of temperature. The values of the other catalysts can be found in the SI. At high temperatures (> 280 °C) experimental data fits well with the theoretical data for FeCuZnK. The pure iron catalyst demonstrates a slightly stronger deviation here. Hence, the equilibrium of the RWGS is then always reached. Decreasing the temperature leads to lower values of the experimental ratio compared to the equilibrium value theoretically predicted

This difference between the "real" theoretical and the experimental "equilibrium" (basically reflecting the deviation from equilibrium) indicates, as expected, that the RWGS reaction is closer to equilibrium at high but not at lower temperatures.

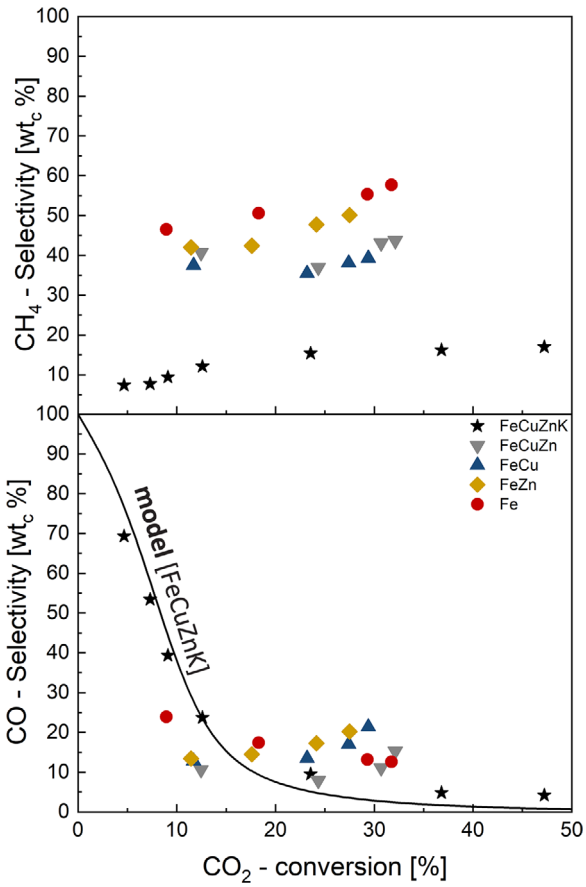

Figure 7. Influence of CO_2 conversion on CH_4 and CO selectivity. Variation of the reaction temperature in 4 steps (220 °C–250 °C–280 °C–300 °C) with constant τ_{mod} for each temperature. Reaction conditions: $m_{cat} = 7.5$ g, $\frac{H_2}{CO_2} = 3(\frac{n}{n})$, TOS ≈ 24 h, $p = 20$ bar, $\tau_{mod,220°C} \approx 50{,}000\ kg_{Kat}sm^{-3}$, $\tau_{mod,300°C} \approx 45{,}000\ kg_{Kat}sm^{-3}$.

The RWGS reaction is therefore at low temperatures kinetically too slow compared to the FTS, but at high temperatures (here >280 °C), the preequilibrium of the RWGS is almost reached for the catalysts.

This can also be seen in Fig. 7 (bottom graph): The CO selectivity and thus CO concentration for the 100Fe15Cu5Zn5K catalyst continue to decrease at higher CO_2 conversions. At 300 °C and a CO_2 conversion of 47%, the CO selectivity is only 4 wt_C%. The CO selectivities of the other catalysts remain almost constant or even increase slightly throughout an increasing CO_2 conversion. For example, the CO selectivity of the 100Fe15Cu catalyst increases from 13% ($X_{CO_2} = 12\%$) to 21% ($X_{CO_2} = 29\%$). Only the pure iron catalyst shows similar results to the potassium-promoted catalyst; that is, the CO selectivity decreases with increasing CO_2 conversion. Similar results for S_{CO} as a function of X_{CO_2} can be found in Refs. [20, 21].

This could also be an indicator for the oxidation of these catalysts or their carbide phases to iron oxides by the high concentrations of water. Iron oxides exhibit a higher RWGS activity in comparison to iron carbides [22]. An increase in the iron

 © 2025 The Author(s). Chemical Engineering & Technology published by Wiley-VCH GmbH

15214125, 2025, 4, Downloaded from https://onlinelibrary.wiley.com/doi/10.1002/ceat.12010 by Universitaet Bayreuth, Wiley Online Library on [10/03/2026]. See the Terms and Conditions (https://onlinelibrary.wiley.com/terms-and-conditions) on Wiley Online Library for rules of use; OA articles are governed by the applicable Creative Commons License

oxide phase is accompanied by a reduction in the iron carbide phase, which suggests that a greater proportion of CO remains in the system and is unable to participate in the conversion process.

There is also a notable difference in the methane selectivity for the potassium-promoted catalyst compared to the other catalysts. The FeCuZnK catalyst shows—for example—a significant lower CH_4 selectivity (19 wt_C% at 300 °C). Wang et al. showed similar CH_4 selectivities and proposed that a promotion with K up to 5 wt% significantly enhances the CO_2 conversion and lowers the CH_4 selectivity due to an increased electron density around the Fe species [5]. The fact that the CH_4 selectivity remains constant during an increase in CO_2 conversion, despite a significant decrease in CO selectivity, indicates that the CH_4 formation is not closely linked to CO formation, as Wang et al. also showed [20]. Since methane is an unwanted side product of the FTS, the 100Fe15Cu5Zn5K catalyst is the optimal choice for use at both low and high FT temperatures.

Furthermore, at 300 °C the potassium promoted catalyst still shows high selectivities toward C_2–C_4 products (around 47 wt_c% → 20 wt_c% olefins) and also for C_{5+} hydrocarbons (approx. 26 wt_c%) and only minimal methanol selectivities (approx. 4 wt_c%). It has been reported that higher olefin selectivities of up to 50 wt% can be achieved at elevated temperatures [18, 23]. This is presumably due to the significantly higher potassium content (10-20 wt%). However, the selectivity to methane is generally higher and the proportion of long chain products is lower, probably due to the effect mentioned in Section 3.1.

The 100Fe15Cu5Zn5K catalyst has been identified as the optimal catalyst for the synthesis of liquid hydrocarbons, as it still achieves an α of 0.58 even at elevated temperatures and high carbon dioxide conversions.

4 Conclusion

In this study, iron-based catalysts were synthesized, characterized, and investigated for their activity and selectivity in the process of low temperature CO_2 conversion to HCs. The properties of the different promoters (Cu, Zn, and K) were determined by varying three factors: the CO_2/CO reactant ratio, the temperature (220 °C–300 °C) and the CO_2 conversion.

All studies have identified that 100Fe15Cu5Zn5K exhibits the lowest methane selectivity and the highest selectivities to the desired long-chain hydrocarbons (C_{5+}) and olefins. The CO_2 conversion variation also indicates that potassium presumably inhibits the oxidation of iron carbides to iron oxides, thereby enabling higher CO_2 conversions. Further studies on the catalyst properties and the influence of H_2O on the iron phases (iron oxides, iron carbides) using, for example, in situ XRD analysis during the reaction are therefore essential to maximize the CO_2 conversion.

In addition, a kinetic model was created using the FeCuZnK catalyst with an LHHW approach. This model serves as a foundation for subsequent kinetic adjustments with regard to the catalyst composition, the reactant ratio, as well as pressure and temperature variations. Nevertheless, in experiments with pure H_2/CO_2 (X_{CO_2} variation) and studies with varying CO_2/CO rations, the model demonstrated a high degree of correlation with the experimental data for CO_2 conversion, CO selectivity and the respective reaction rates.

Supporting Information

Supporting information for this article can be found under DOI: https://doi.org/10.1002/ceat.12010.

This section includes additional references to primary literature relevant for this research [24–26].

Acknowledgments

Open access funding enabled and organized by Projekt DEAL.

Symbols used

a_{H20}	[–]	H_2O inhibition parameter for the kinetic model
b_{CO2}	[–]	CO_2 inhibition parameter for the kinetic model
c_{CO}	[–]	CO inhibition parameter for the kinetic model
c	[mol m^{-3}]	Molar concentration
E_A	[kJ mol^{-1}]	Activation energy
K_{eq}	[–]	Equilibrium constant
k_0	[m^3 s^{-1} kg$_{cat}$$^{-1}$]	Preexponential factor
k	[m^3 s^{-1} kg$_{cat}$$^{-1}$]	Reaction rate constant
$\dot{n}$	[mol h^{-1}]	Mole flow
m_{Cat}	[kg]	Catalyst mass
r	[mmol s^{-1} kg$_{Cat}$$^{-1}$]	Reaction rate
S	[wt_c%]	Selectivity
T	[°C]	Temperature
p	[bar]	Pressure
X	[%]	Conversion
x	[–]	Mole fraction
Z	[–]	Mole fraction of product produced via α_1-distribution

Greek letters

α	[–]	Chain growth probability
τ_{mod}	[kg s m^{-3}]	Modified residence time
ξ	[–]	Break point, C-number

Abbreviations

FTS	Fischer–Tropsch synthesis
GC	Gas chromatography
HCs	Hydrocarbons
IR	Infrared

 © 2025 The Author(s). Chemical Engineering & Technology published by Wiley-VCH GmbH

15214125, 2025, 4, Downloaded from https://onlinelibrary.wiley.com/doi/10.1002/ceat.12010 by Universitaet Bayreuth, Wiley Online Library on [10/03/2026]. See the Terms and Conditions (https://onlinelibrary.wiley.com/terms-and-conditions) on Wiley Online Library for rules of use; OA articles are governed by the applicable Creative Commons License

PTL	Power-to-liquid
RWGS	Reverse-water-gas shift
STP	Standard temperature and pressure
TCD	Thermal conductivity detector
TOS	Time on stream
WGS	Water-gas shift

References

[1] T. Bayer, in *CO_2 and CO as Feedstock* (Eds: M. Kircher, T. Schwarz), *Circular Economy and Sustainability*, Springer International Publishing, Cham **2023**.

[2] C. Panzone, R. Philippe, A. Chappaz, P. Fongarland, A. Bengaouer, *J. CO_2 Util.* **2020**, *38*, 314–347. DOI: https://doi.org/10.1016/j.jcou.2020.02.009

[3] A. Jess, P. Wasserscheid, *Chemical Technology: From Principles to Products*, John Wiley & Sons, Weinheim, Germany **2020**.

[4] M. V. Landau, N. Meiri, N. Utsis, R. Vidruk Nehemya, M. Herskowitz, *Ind. Eng. Chem. Res.* **2017**, *56* (*45*), 13334–13355. DOI: https://doi.org/10.1021/acs.iecr.7b01817

[5] Q. Wang, K. Hu, R. Gao, L. Zhang, L. Wang, C. Zhang, *Atmosphere* **2022**, *13* (*8*), 1238. DOI: https://doi.org/10.3390/atmos13081238

[6] T. Riedel, H. Schulz, G. Schaub, K.-W. Jun, J.-S. Hwang, K.-W. Lee, *Top. Catal.* **2003**, *26* (*1-4*), 41–54. DOI: https://doi.org/10.1023/B:TOCA.0000012986.46680.28

[7] T. Riedel, G. Schaub, K.-W. Jun, K.-W. Lee, *Ind. Eng. Chem. Res.* **2001**, *40* (*5*), 1355–1363. DOI: https://doi.org/10.1021/ie000084k

[8] *Chemierohstoffe aus Kohle: Mit 168 Tabellen* (Eds: J. Falbe, E. Ahland), Thieme Verlag, Stuttgart **1977**.

[9] G. H. Graaf, P. Sijtsema, E. J. Stamhuis, G. Joosten, *Chem. Eng. Sci.* **1986**, *41* (*11*), 2883–2890. DOI: https://doi.org/10.1016/0009-2509(86)80019-7

[10] W. Ning, N. Koizumi, M. Yamada, *Energy Fuels* **2009**, *23* (*9*), 4696–4700. DOI: https://doi.org/10.1021/ef900428t

[11] P. S. Sai Prasad, J. W. Bae, K.-W. Jun, K.-W. Lee, *Catal. Surv. Asia* **2008**, *12* (*3*), 170–183. DOI: https://doi.org/10.1007/s10563-008-9049-1

[12] M Dry, *J. Catal.* **1969**, *15* (*2*), 190–199.

[13] P. H. Choi, K.-W. Jun, S.-J. Lee, M.-J. Choi, K.-W. Lee, *Catal. Lett.* **1996**, *40* (*1-2*), 115–118. DOI: https://doi.org/10.1007/BF00807467

[14] W. Wang, X. Jiang, X. Wang, C. Song, *Ind. Eng. Chem. Res.* **2018**, *57* (*13*), 4535–4542. DOI: https://doi.org/10.1021/acs.iecr.8b00016

[15] X. Chen, R. Gao, Q. Wang, K. Hu, F. Wang, C. Deng, L. Xu, C. Zhang, K.-W. Jun, S. Ki Kim, T. Zhao, H. Wan, G. Guan, *Fuel* **2024**, *364*, 131061. DOI: https://doi.org/10.1016/j.fuel.2024.131061

[16] P. H. Choi, K.-W. Jun, S.-J. Lee, M.-J. Choi, K.-W. Lee, *Catal. Lett.* **1996**, *40* (*1-2*), 115–118. DOI: https://doi.org/10.1007/BF00807467

[17] K. Nasriddinov, J.-E. Min, H.-G. Park, S. J. Han, J. Chen, K.-W. Jun, S. K. Kim, *Catal. Sci. Technol.* **2022**, *12* (*3*), 906–915. DOI: https://doi.org/10.1039/D1CY01980E

[18] S.-M. Hwang, S. J. Han, J. E. Min, H.-G. Park, K.-W. Jun, S. K. Kim, *J. CO_2 Util.* **2019**, *34*, 522–532. DOI: https://doi.org/10.1016/j.jcou.2019.08.004

[19] M. Claeys, E. van Steen, T. Botha, R. Crous, A. Ferreira, A. Harilal, D. J. Moodley, P. Moodley, E. Du Plessis, J. L. Visagie, *ACS Catal.* **2021**, *11* (*22*), 13866–13879. DOI: https://doi.org/10.1021/acscatal.1c03719

[20] W. Wang, X. Wang, G. Zhang, K. Wang, F. Zhang, T. Yan, J. T. Miller, X. Guo, C. Song, *Front. Chem. Eng.* **2021**, *3*, 708014. DOI: https://doi.org/10.3389/fceng.2021.708014

[21] C. Panzone, R. Philippe, C. Nikitine, L. Vanoye, A. Bengaouer, A. Chappaz, P. Fongarland, *Ind. Eng. Chem. Res.* **2021**, *60* (*46*), 16635–16652. DOI: https://doi.org/10.1021/acs.iecr.1c02542

[22] M. E. Dry, in *Catalysis*. Vol. *1* (Ed: H. Heinemann), 2021st ed., De Gruyter, Berlin/Boston **2022**.

[23] J. Zhang, S. Lu, X. Su, S. Fan, Q. Ma, T. Zhao, *J. CO_2 Util.* **2015**, *12*, 95–100. DOI: https://doi.org/10.1016/j.jcou.2015.05.004

[24] A. Seidel, *Fischer-Tropsch-Synthese zur selektiven Erzeugung von Flugturbinenekraftstoff, Diploma*, University of Bayreuth **2013**.

[25] T. J. Donnelly, I. C. Yates, C. N. Satterfield, *Energy Fuels* **1988**, *2* (*6*), 734–739. DOI: https://doi.org/10.1021/ef00012a003

[26] G. A. Huff, C. N. Satterfield, *Ind. Eng. Chem. Proc. Des. Dev.* **1985**, *24* (*4*), 986–995. DOI: https://doi.org/10.1021/i200031a015

 © 2025 The Author(s). Chemical Engineering & Technology published by Wiley-VCH GmbH

15214125, 2025, 4, Downloaded from https://onlinelibrary.wiley.com/doi/10.1002/ceat.12010 by Universitaet Bayreuth, Wiley Online Library on [10/03/2026]. See the Terms and Conditions (https://onlinelibrary.wiley.com/terms-and-conditions) on Wiley Online Library for rules of use; OA articles are governed by the applicable Creative Commons License